Investigation of Rod-shaped Single Graphene Quantum Dot

Hugo Levy-Falk, Océane Capelle, Thomas Liu, Emmanuelle Deleporte, Loïc Rondin, Jean-Sébastien Lauret, Daniel Medina-Lopez, Stéphane Campidelli

Investigation of Rod-shaped Single Graphene Quantum Dot

*Hugo Levy-Falk Océane Capelle Thomas Liu Daniel Medina-Lopez Emmanuelle Deleporte Stéphane Campidelli Loïc Rondin Jean-Sébastien Lauret**

H. Levy-Falk, O. Capelle, Dr. T. Liu, Prof. E. Deleporte, Dr. L. Rondin, Prof. JS Lauret
LUMIN, Université Paris Saclay, ENS Paris Saclay, CentraleSupelec, CNRS, Orsay, France
Email Address:lauret@ens-paris-saclay.fr
Dr. D. Medina-Lopez, Dr. S. Campidelli
Université Paris-Saclay, CEA, CNRS, NIMBE, LICSEN, 91191 Gif-sur-Yvette, France

Keywords: *Nanographene, quantum dot, single photon*

In recent years, there has been a resurgence of interest in graphene quantum dots (*i.e.* large polycyclic aromatic hydrocarbons) in particular due to their interesting properties as single quantum emitters. Here, we report on a thorough study of a graphene quantum dot made of 96 carbon atoms in a D_{2h} symmetry. In particular, experiments at the single molecule level reveal that this graphene quantum dot structure is a bright and photo-stable single photon emitter at room temperature. Finally, a statistical study of the emission wavelength as a function of the graphene quantum dot concentration highlights the high purity and degree of control on the samples.

1 Introduction

Graphene Quantum Dots (GQDs), large polycyclic aromatic hydrocarbons (PAHs) with ∼100 sp^2 carbon atoms or more, are a promising platform for many applications. Among many examples, GQDs films can exhibit amplified spontaneous emission [1], near-infrared lasing [2], or be stable quantum light emitters [3, 4]. Many synthesis methods have been proposed for GQDs, often classified between "top-down" and "bottom-up" routes [5]. These can be complemented by post-synthetic modification and functionalization, for example, to protect carbon dots from degradation [6]. Among the challenges of using GQDs for single-molecule applications, aggregation of the dots can alter their properties significantly [7]. Bottom-up synthesis is of peculiar interest for the study of fundamental properties of GQDs, as it yields quantum dots with well-defined structure and size. Recently, we reported on a new bottom-up synthesis of rod-shaped GQDs with a number of carbon atoms ranging from 78 to 132 [8]. Bulky *tert*-butyl groups have been added at specific locations on the structure leading to a drastic enhancement of the solubility, in contrast to our previously reported triangular GQDs [9], thus allowing the use of standard purification techniques to remove by-products such as chlorinated materials of incompletely oxidized GQDs. As a result, purified samples of $\mathbf{C_{96}}\boldsymbol{t}\mathbf{Bu_8}$ are obtained, characterized by a very clean photo-luminescence (PL) spectrum in solution and a photo-luminescence quantum yield (PLQY) as high as ∼95 %. Harvesting the full potential of these properties and attempting any more complex experiment with those GQDs requires single-molecule characterization.

This paper focuses on the single-molecule characterization of the $\mathbf{C_{96}}\boldsymbol{t}\mathbf{Bu_8}$ GQD. We show that it can be a very photo-stable single photon emitter at room temperature. Then, performing statistics on samples with various concentrations in the original solution, we study the purity of the synthesized samples and highlight the low amount of by-product impurities and aggregates.

2 Results and discussion

2.1 Optical properties of $C_{96}tBu_8$ in solution

The structure of $\mathbf{C_{96}}\boldsymbol{t}\mathbf{Bu_8}$ is shown in Figure 1a. Powders of such compounds can be dissolved in organic solvents, such as 1,2,4 trichlorobenzene (TCB) or tertahydrofuran (THF). Figure 1b shows the absorption spectrum, photoluminescence spectrum, and photoluminescence excitation spectrum (PLE)

of a solution of $\mathbf{C_{96}tBu_8}$ in THF. A sharp zero-phonon line (ZPL) at 2.058 eV is observed in the absorption spectrum, which also displays the vibrational progression corresponding to the main absorption bands. The peaks at 2.222 eV and 2.262 eV correspond to the vibronic (0-1) replica of the zero-phonon that we attribute to molecular vibrations at 170 and 200 meV resulting from linear combinations of localized vibrations of carbon-carbon bonds [8]. The second singlet transition band is also visible at 2.69 eV and features the same vibronic replica. The sharp features present in the absorption spectrum make $\mathbf{C_{96}tBu_8}$ standing out among previously reported GQDs where the absorption of aggregates dominates the spectra [9, 10, 11]. We measured the molar extinction coefficient of $\mathbf{C_{96}tBu_8}$ in THF solution at the second band to 488 760 $M^{-1}{\cdot}cm^{-1}$, which corresponds to an effective cross-section of ~ 18 $Å^2$ and equivalent to $\sim 2.10^{-17}$ cm^2/carbon atom. This value is comparable to the absorption cross-sections at the second excitonic transition measured for carbon nanotubes [12].
The photoluminescence spectrum shown in Figure 1b features a sharp zero-phonon line at 2.026 eV. The corresponding Stokes shift is 32 meV, which is on-par with smaller PAHs, *e.g.*, perylene (35 meV) [13]. Two vibronic replicas at ∼170 meV complete the mirror symmetry. This spectrum is typical for the emission from GQDs monomers [9, 3]. It is worth mentioning that almost no emission is observed at higher energy in contrast with our previous report on triangle-shaped $\mathbf{C_{96}(C_{12}H_{25})_6}$ [14]. This is related to the solubility and purity of this family of GQDs [8]. The excitation spectrum, collected on the edge of the zero-phonon line, is shown in Figure 1b. The spectrum perfectly matches the absorption spectrum, which confirms that GQDs are highly individualized in the solution. Indeed, since the emission spectrum is associated with emission from monomers, the good overlap of excitation and absorption spectra means that the species absorbing are the same as the ones emitting.
Time-resolved photoluminescence traces reported in Figure 1c further confirm these results. Both measurements, collected at 1.99 eV and 1.84 eV, are characterized by an almost mono-exponential decay with a characteristic decay time of ∼2.82 ns. A second exponential with low fractional contribution (around 6 %) and a lifetime of 10.1 ns is needed to fit the decay curve [15]. This almost mono-exponential decay advocates for an emission spectrum that originates almost solely from one species of emitters.

2.2 Photoluminescence properties of single $C_{96}tBu_8$ in PS matrix

The single-molecule study was conducted on thin polystyrene films doped with $\mathbf{C_{96}tBu_8}$ at different concentrations and at room temperature. Samples were prepared as described in the experimental section. Figure 2a shows a raster confocal fluorescence scan excited by a 594 nm laser (2.087 eV). Diffraction-limited spots were selected for spectroscopy studies.
First, second-order correlation measurements ($g^{(2)}(\tau)$) under continuous illumination were performed using a homemade Hanbury Brown and Twiss interferometer. Figure 2c gives a typical histogram for a correlation measured under 0.15 kW/cm² excitation with the corresponding fitted $g^{(2)}(\tau)$. The fit yielded $g^{(2)}(\tau = 0) = 0.17$, which is a precise indicator for single-photon emitters [16]. Note here that no background subtraction has been done. Rise-time was fitted to 2.43 ns, which is shorter than the lifetime in solution (2.82 ns). This is expected for a single emitter under continuous excitation, as the laser increases the effective transition rate [17]. Moreover, Figure 2c displays bunching ($g^{(2)}(\tau) > 1$) at $\tau \neq 0$, which we attribute to the presence of a meta-stable triplet state that lies below the first singlet excited state [17].
A typical photoluminescence spectrum from a single $\mathbf{C_{96}tBu_8}$ is shown in Figure 2b. The emission spectrum is well-fitted using three Lorentzian profiles centered here at 2.00 eV, 1.83 eV, and 1.66 eV, respectively. We investigate later the variations in ZPL energy. The energy gap $\Delta E_{1-2;2-3}$ between lines is 170 meV, similar to the ones in solution.
Figure 2d is a polarization diagram reporting emission and excitation scans for a single $\mathbf{C_{96}tBu_8}$. It shows that emission and absorption from a single $\mathbf{C_{96}tBu_8}$ are linearly polarized and that absorption and emission dipoles share the same direction. This confirms the theoretical predictions and anisotropy measurements in solution previously reported [8].
A typical time trace at low excitation intensity (0.15kW/cm^2) is shown in Figure 2e. A signal-to-noise ratio (SNR) of 9.16 is measured. The excellent agreement with the expected theoretical SNR ($\sim$ 9.53)

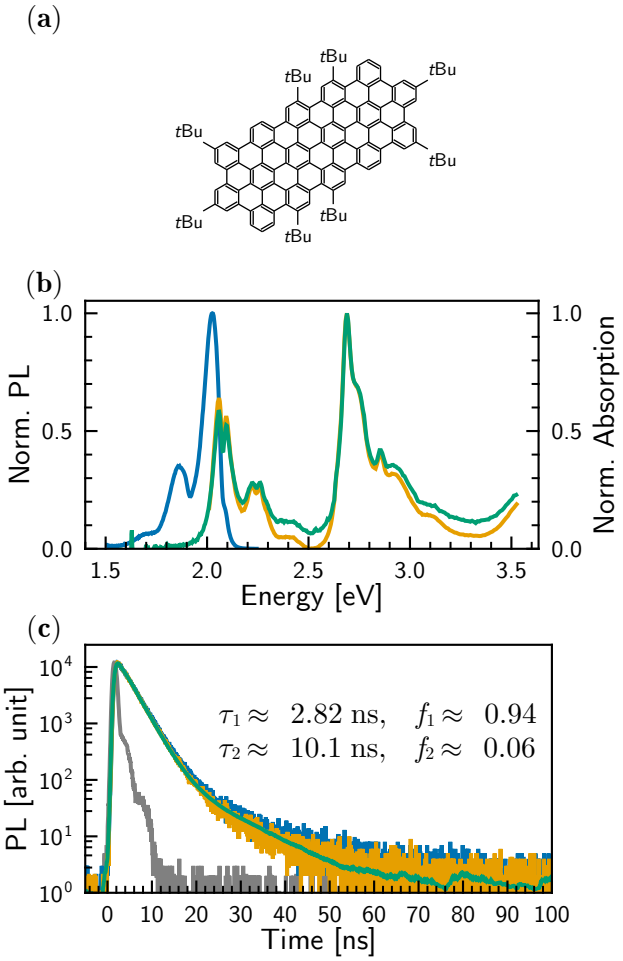

Figure 1: (a) Chemical structure of $\mathbf{C_{96}tBu_8}$. *t*Bu: *tert*-butyl.(b) Absorption spectrum (solid green line), photoluminescence spectrum excited at 2.69 eV (solid blue line) and excitation spectrum collected at 1.99 eV (solid yellow line) in THF. Excitation and absorption spectra superimpose neatly, hinting at no aggregation in the sample. (c) Time-resolved photoluminescence traces collected around the zero-phonon line at 1.99 eV (solid blue line) and around the first phonon replica at 1.84 eV (solid yellow line) in TCB. The instrument response function is in grey. Decays were fitted with two exponential (solid green line), yielding lifetimes of 2.82 and 10.1 ns, respectively. f_i indicates fractional contribution [15] of component i.

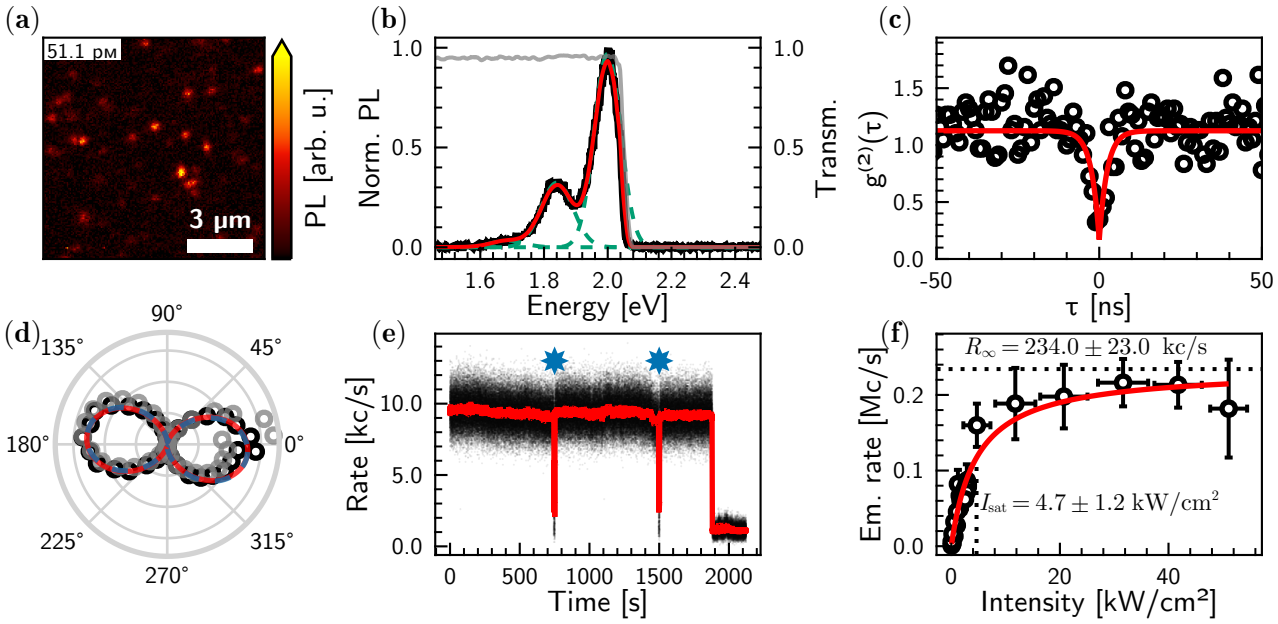

Figure 2: (a) Confocal raster scans of sample with $\mathbf{C_{96}tBu_8}$ in PS matrix displaying diffraction-limited emission spots. Concentration in the solution was 54.6 pM. (b) Typical PL spectrum of a single $\mathbf{C_{96}tBu_8}$ (solid black), with the corresponding fitted model (solid red). The model includes setup transmission (solid light gray) and three Lorentzian peaks (dashed green). (c) Second-order correlation measurement, excited at 0.15 kW/cm^2. The histogram (black circles) is fitted using a single exponential with a constant added to account for bunching (solid red line). $g^{(2)}(\tau)$ at origin is fitted at 0.17, and the characteristic time of the exponential is 2.43 ns. (d) Emission polarization diagram (black circles) fitted with Malus's law (solid red line) and excitation polarization scan (grey circles) fitted with Malus's law (dashed blue line). The two fit superimpose nearly perfectly. (e) Time trace of the measured emission of a single emitter at excited at 0.15 kW/cm^2. Binning rate is 100 Hz. The moving average over 2 s is plotted in solid red. Manual adjustments of the setup are marked with a blue star. Other variations are attributed to experimental instabilities. (f) Saturation curve of a single $\mathbf{C_{96}tBu_8}$ (black circles). The curve is fitted to the model in equation 1, yielding a saturation intensity of 4.7 ± 1.2 kW/cm^2 and an asymptotic rate of 234 ± 23 kc/s. Signals for Figures (c), (d), (e) and (f) are collected over the whole spectrum in Figure (b)

demonstrates that our measurement is shot noise limited. We also stress that no blinking was recorded for binning rate used (100 Hz) and that the photon count rate remains constant under continuous illumination for up to thirty minutes, demonstrating that $\mathbf{C_{96}tBu_8}$ GQDs in the PS matrix are remarkably stable, despite that no particular precaution has been taken to reach this result. Thus, we foresee that GQDs stability can even be increased by a careful choice of matrix and preparation steps.
The high stability of single $\mathbf{C_{96}tBu_8}$ allows for intensity saturation measurements. Figure 2f shows the emission rate of a single $\mathbf{C_{96}tBu_8}$ estimated from our setup transmission for various excitation intensities. Given the observed bunching in the $g^{(2)}$ measurement, we model the $\mathbf{C_{96}tBu_8}$ by a three-levels system leading to an emission rate written as

$$R = R_\infty \frac{1}{1 + I_{\text{sat}}/I}\,, \tag{1}$$

where R_∞ is the emission rate for infinitely high excitation intensity, I is the excitation intensity, and I_{sat} the saturation intensity. Fitting this model to the data in Figure 2f yields a saturated emission rate R_∞ of 234 ± 23 kc/s and a saturation intensity I_{sat} of 4.7 ± 1.2 kW/cm^2. This saturated emission rate is in good agreement with the excellent quantum efficiency measured in the solution and the collection efficiency of our setup.

2.3 Statistical study of diffraction-limited emitters.

Sample preparation is a crucial step in single-molecule experiments, mainly because impurities with emission spectra similar to the object of interest can make it challenging to ensure the right single-molecule

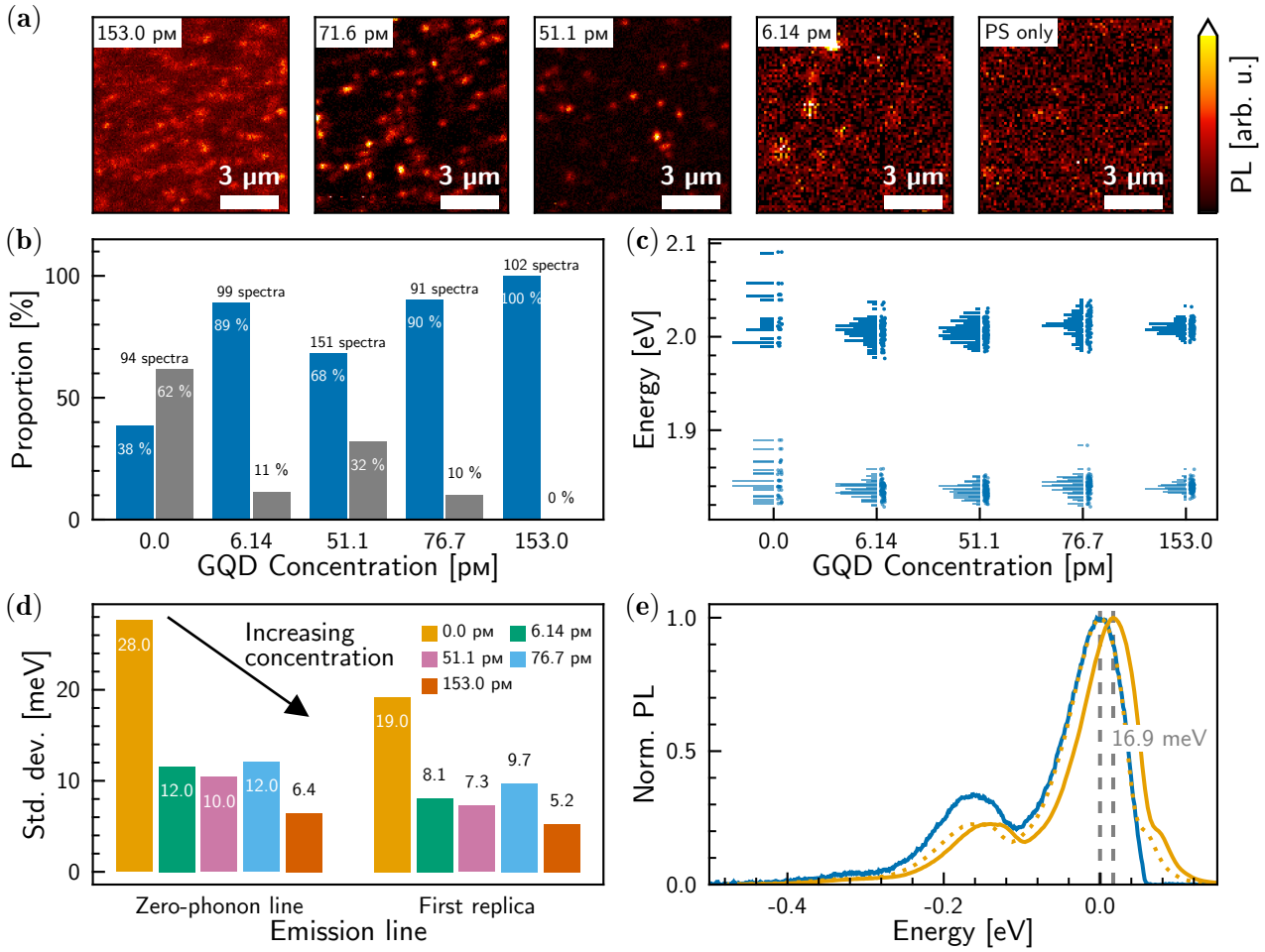

Figure 3: (a) Confocal raster scans of four films with decreasing GQD concentration in the solution and reference sample with PS matrix only. (b) Proportion of successfully (dark blue) and unsuccessfully (gray) fitted spectra observed in films against the concentration of $\mathbf{C_{96}tBu_8}$ in the solution. (c) Distribution of position of the zero-phonon line (dark blue) and first vibronic replica (light blue) emission peaks of successfully fitted spectra. (d) Evolution of the standard deviation of the peaks' distribution for the concentrations of solution studied. (e) Comparison of the PL spectrum from a solution of $\mathbf{C_{96}tBu_8}$ (solid yellow line) and the sum of all PL spectra from our most concentrated PS sample, 164 pM (102 spectra, solid blue line). Energies are centered around the ZPL of the averaged spectrum (2.016 eV). The dotted yellow line is the spectrum in solution shifted by 9.4 meV, so ZPL is at 0 eV to compare its line width with that of the averaged spectrum.

is being observed. This problem has been raised in several studies, and different hypotheses have been proposed for the origin of those impurities, ranging from solvent impurities [18] to organic impurities from the caps of glass vials [19], impurities in polymer matrices [11], or defects in silica [20]. A thorough investigation of fluorescent impurities in our single-molecule experiments can be found in references [14, 9, 21]. Here, we demonstrate the high purity of our samples, making $\mathbf{C_{96}tBu_8}$ an ideal platform to conduct single-molecule experiments.

To highlight the high purity of the synthesized $\mathbf{C_{96}tBu_8}$ powders, we conducted a statistical study of emission spectra from light emitters present in the PS matrix against the concentration of $\mathbf{C_{96}tBu_8}$ in the original solution. We prepared samples with various concentrations of $\mathbf{C_{96}tBu_8}$, ranging from 7.0 pM to 170 pM, and a control sample without GQDs. As expected, the density of emitters available on a confocal scan decreases with lower concentrations of $\mathbf{C_{96}tBu_8}$ in the solution, as shown in Figure 3a. Spectra were classified using a simple three-emission-peaks model, following the method described in the experimental section. An example of a fit result is shown in Figure 2b. The proportion of spectra successfully fitted by the model increases with higher concentrations of GQDs, as shown in Figure 3b. This means that the number of potential $\mathbf{C_{96}tBu_8}$ in the sample increases as the concentration of the solution is increased.

To further ensure that the spectra successfully fitted by the model correspond to $\mathbf{C_{96}tBu_8}$, the central

emission energy of zero-phonon and first vibronic replica emission peaks were then grouped by sample concentration and binned to form histograms such as presented in Figure 3c. These histograms show that from a seemingly uniform distribution of central emission energy, the histograms look more and more like a normal distribution when concentration increases. We then calculated the standard deviation for each set of ZPL associated with a concentration. Figure 3d shows the evolution of the standard deviation of histograms for both emission peaks. It is clear that the standard deviation decreases as $\mathbf{C_{96}tBu_8}$ concentration increases, hinting that all emitters added in the polystyrene matrix, when increasing concentration, have approximately the same emission energy.
From the evolution of the ratio of successfully fitted spectra and the decreasing standard deviations shown in Figure 3d, we see that increasing the concentration in the solution before spin-coating mainly increases the concentration of $\mathbf{C_{96}tBu_8}$ in the film. Another phrasing of this last affirmation is that fluorescent impurities in our samples do not arise from residual compounds from the synthesis of GQDs. The remaining possible impurities sources are thus substrate degradation, polymer matrix, and impurities from the solvent.
As most of the emitters in the most concentrated sample appear to be $\mathbf{C_{96}tBu_8}$, it makes sense to link the emission spectrum of those emitters to the emission spectrum in solution. Figure 3e shows the emission spectrum in solution as well as the mean of all 102 emission spectra recorded on our most concentrated sample (164 pM). Both spectra have the same general features and, despite a $\sim$ 15 meV redshift of the averaged spectrum, the same line widths. We attribute this red shift to solvatochromism. As emission in the solution originates from individualized emitters, and because the distribution of ZPL is very narrow, the similar line widths of the averaged spectrum and the spectrum in solution show that the broadening in the emission spectrum of the solution is mostly homogeneous.

3 Conclusion

We have performed a statistical study of newly reported GQDs, $\mathbf{C_{96}tBu_8}$, at the single-molecule level. We show that $\mathbf{C_{96}tBu_8}$ GQDs are bright and stable single photons emitters at room temperature. Furthermore, we confirmed the theoretical predictions of aligned excitation and emission dipoles for the first singlet transition of the GQD. The statistical study as a function of the GQDs concentration shows a decrease of the standard deviation of 0-0 transition energy when concentration increases. It shows that a large majority of the added emitters are indeed $\mathbf{C_{96}tBu_8}$ GQDs and that almost no emitting by-products are present in the sample highlighting its high purity.
Prospects for this family of GQDs include ultra-fast investigation of the internal conversion dynamics as a function of the number of carbon atoms. Moreover, their good stability, high quantum yield, and one-atom thickness make them desirable candidates for quantum sensing applications. In particular, it is planned to use them to probe the surface properties of active materials.

4 Experimental Section

Characterization of $\boldsymbol{C_{96}tBu_8}$ *in solution*: Rod-shaped $\mathbf{C_{96}tBu_8}$ GQDs were synthesized and characterized as previously reported [8]. They were then dispersed in spectroscopic-grade tetrahydrofuran purchased from Thermo Scientific. The concentration of GQDs was assessed through the absorption spectrum of the solution using an FS5 spectrofluorometer from Edinburgh Instruments. Further dilutions allowed getting the expected concentration of GQDs.
The molar extinction coefficient was assessed by dispersing a known mass of $\mathbf{C_{96}tBu_8}$, measured with a micro-balance, in THF. Absorption spectra were then acquired for diluted solutions.

Preparation and characterization of $\boldsymbol{C_{96}tBu_8}$ *embedded in polystyrene films*:
A solution with 10 % w.r.t. of polystyrene in THF is then prepared. The solution was heated at 75 °C for 30 minutes to dissolve the polystyrene beads completely. Both solutions are then mixed in equal vol-

Table 1: Input parameters for Levenberg-Marquardt algorithm. HWHM, Half Width Half Maximum.

Peak	Norm. Amplitude			Center [eV]			HWHM [meV]		
	Init.	Min.	Max.	Init.	Min.	Max.	Init.	Min.	Max.
1	1	0	$+\infty$	2.0	1.90	2.10	100	6	162
2	1/3	0	$+\infty$	1.83	1.75	1.9	100	6	138
3	0.1	0	$+\infty$	1.67	1.55	1.75	50	10	250

umetric quantities. Reported concentrations in this work correspond to the calculated concentration of GQDs in the resulting solution.
The films were then prepared by spin-coating the mixture on glass substrates (Schott Nexterion). The substrates were plasma-cleaned for 20 minutes beforehand. The rotation speed was 1000 rpm, acceleration 500 rpm/s, and rotation time 180 s. The samples were dried on a hot plate (90 °C) for 1 h. The resulting films were 1 to 2 µm thick, measured with a profilometer.

Confocal microscopy and spectroscopy:
Single-molecule experiments were performed at room temperature on a homemade confocal microscope. Samples are excited using a 594 nm c.w. laser (Cobolt Mambo 100) focused by a microscope objective (0.95 NA MPLAPON100X M Plan Apochromat objective from Evident Scientific). Photoluminescence from the sample is collected through the same lens. A laser beam splitter separates excitation and emission beams (zt 594 RDC, Chroma). Emission from the sample is then spatially filtered through a 75 µm pin-hole, and residual light from the laser is filtered using a Thorlabs FELH0600 filter. Transmission resulting from filters is reproduced from manufacturer data in Figure 2b (light gray). Detection is performed using either silicon avalanche photodiodes (SPCM-AQR-13, Excelitas) for raster scans and $g^{(2)}(\tau)$ measurements or a monochromator (SP-2350, Princeton Instruments) with an LN-cooled CCD camera (PyLoN:100BR eXcelon, Princeton Instruments) for spectral measurements. Raster scans are recorded using a dedicated acquisition card (PCIe-6323, National Instruments) and a Python-based suite for experiment control [22]. $g^{(2)}(\tau)$ acquisition was performed thanks to a TCSPC card (Swabian Time Tagger 20).

Semi-automatic treatment of PL spectra:
To ensure reliable and reproducible statistics on the distribution of peak emission wavelength, recorded spectra were fitted with a model comprising three Lorentzian peaks and the transmission of the setup based on manufacturer data for the dichroic mirror and clean-up filter. The model was fitted on each normalized spectrum using the Levenberg–Marquardt algorithm with the input parameters given in Table 1, and data points outside the transmission region of the filter were given a null weight. Spectra were post-selected to remove fit results that would be difficult to interpret, including flat ones, which correspond to impurities burning quickly. All treatments were performed using the Julia programming language [23]. All data visualizations within this paper were plotted using the Makie.jl library [24].

Supporting Information
Supporting Information is available from the Wiley Online Library or from the author.

Acknowledgements
The authors acknowledge financial support from the Ministry of Armies (Agence de l'innovation de défense). This work has been financially supported by the FLAG-ERA Grant OPERA by DFG 437130745 and ANR-19-GRF1-0002-01, by the ANR-DFG NLE Grant GRANAO ANR-19-CE09-0031-01, ANR grant DELICACY ANR-22-CE47-0001-03, ANR grant GANESH ANR-21-CE09-0025, by a public grant overseen by the French National Research Agency (ANR) as part of the "Investissements d'Avenir" program (Labex NanoSaclay, reference: ANR-10-LABX-0035).

References

[1] X. Xu, G. Serra, A. Villa, R. Muñoz-Mármol, S. Vasylevskyi, M. Gadea, A. Lucotti, Z. Lin, P. G. Boj, R. Kabe, M. Tommasini, M. Á. Díaz-García, F. Scotognella, G. M. Paternò, A. Narita, *Chem. Sci.* **2022**, *13*, 44 13040.

[2] G. M. Paternò, Q. Chen, R. Muñoz-Mármol, M. Guizzardi, V. Bonal, R. Kabe, A. J. Barker, P. G. Boj, S. Chatterjee, Y. Ie, J. M. Villalvilla, J. A. Quintana, F. Scotognella, K. Müllen, M. A. Díaz-García, A. Narita, G. Lanzani, *Mater. Horiz.* **2022**, *9*, 1 393.

[3] S. Zhao, J. Lavie, L. Rondin, L. Orcin-Chaix, C. Diederichs, P. Roussignol, Y. Chassagneux, C. Voisin, K. Müllen, A. Narita, S. Campidelli, J.-S. Lauret, *Nat. Commun.* **2018**, *9*, 1 3470.

[4] Q. Chen, S. Thoms, S. Stöttinger, D. Schollmeyer, K. Müllen, A. Narita, T. Basché, *J. Am. Chem. Soc.* **2019**, *141*, 41 16439.

[5] Z. Li, L. Wang, Y. Li, Y. Feng, W. Feng, *Mater. Chem. Front.* **2019**, *3*, 12 2571.

[6] P. Long, Y. Feng, C. Cao, Y. Li, J. Han, S. Li, C. Peng, Z. Li, W. Feng, *Adv. Funct. Mater.* **2018**, *28*, 37 1800791.

[7] P. Long, Y. Feng, Y. Li, C. Cao, S. Li, H. An, C. Qin, J. Han, W. Feng, *ACS Appl. Mater. Interfaces* **2017**, *9*, 43 37981.

[8] D. Medina-Lopez, T. Liu, S. Osella, H. Levy-Falk, N. Rolland, C. Elias, G. Huber, P. Ticku, L. Rondin, B. Jousselme, D. Beljonne, J.-S. Lauret, S. Campidelli, *Nat. Commun.* **2023**, *14*, 1 4728.

[9] T. Liu, C. Tonnelé, S. Zhao, L. Rondin, C. Elias, D. Medina-Lopez, H. Okuno, A. Narita, Y. Chassagneux, C. Voisin, S. Campidelli, D. Beljonne, J.-S. Lauret, *Nanoscale* **2022**, *14*, 10 3826.

[10] J. A. McGuire, *Phys. Status Solidi* **2016**, *10*, 1 91.

[11] A. Neumann, J. Lindlau, S. Thoms, T. Basché, A. Högele, *Nano Lett.* **2019**, *19*, 5 3207.

[12] F. Vialla, C. Roquelet, B. Langlois, G. Delport, S. M. Santos, E. Deleporte, P. Roussignol, C. Delalande, C. Voisin, J.-S. Lauret, *Phys. Rev. Lett.* **2013**, *111*, 13 137402.

[13] I. B. Berlman, In I. B. Berlman, editor, *Handbook of Fluorescence Spectra of Aromatic Molecules (Second Edition)*, 107–415. Academic Press, ISBN 978-0-12-092656-5, **1971**.

[14] T. Liu, These de doctorat, université Paris-Saclay, **2023**.

[15] J. R. Lakowicz, In *Principles of Fluorescence Spectroscopy*, 97–155. Springer US, Boston, MA, ISBN 978-0-387-46312-4, **2006**.

[16] L. Novotny, B. Hecht, *Principles of Nano-Optics*, Cambridge University Press, Cambridge, 2 edition, **2012**.

[17] S. Zhao, Ph.D. thesis, Université Paris Saclay (COmUE), **2018**.

[18] L. Fleury, Ph. Tamarat, B. Kozankiewicz, M. Orrit, R. Lapouyade, J. Bernard, *Mol. Cryst. Liq. Cryst. Sci. Technol., Sect. A* **1996**, *283*, 1 81.

[19] V. Tripathi, P. Linga Reddy, L. S. Panchakarla, *ChemPhysChem* **2021**, *22*, 12 1167.

[20] F. T. Rabouw, N. M. B. Cogan, A. C. Berends, W. van der Stam, D. Vanmaekelbergh, A. F. Koenderink, T. D. Krauss, C. d. M. Donega, *Sci. Rep.* **2016**, *6*, 1 21187.

[21] T. Liu, B. Carles, C. Elias, C. Tonnelé, D. Medina-Lopez, A. Narita, Y. Chassagneux, C. Voisin, D. Beljonne, S. Campidelli, L. Rondin, J.-S. Lauret, *J. Chem. Phys.* **2022**, *156*, 10 104302.

[22] J. M. Binder, A. Stark, N. Tomek, J. Scheuer, F. Frank, K. D. Jahnke, C. Müller, S. Schmitt, M. H. Metsch, T. Unden, T. Gehring, A. Huck, U. L. Andersen, L. J. Rogers, F. Jelezko, *SoftwareX* **2017**, *6* 85.

[23] J. Bezanson, A. Edelman, S. Karpinski, V. B. Shah, *SIAM Rev.* **2017**, *59*, 1 65.

[24] S. Danisch, J. Krumbiegel, *JOSS* **2021**, *6*, 65 3349.